Vol. 23, No. 3(2024) Alim24322
Revista Mexicana de Ingeniería Química
Ingeniería de alimentos

Study of drying, thermal, shrinkage, and color kinetics using digital and thermographic imaging of potato slices under real-time convective drying

Estudio de las cinéticas de secado, térmicas, encogimiento y color de rebanadas de papa usando imágenes digitales y termográficas bajo secado convectivo en tiempo real

S.M. Gutiérrez-Martínez[1], J. D. Hernández-Varela[1], J. J. Chanona-Pérez[1]*, J. V. Méndez-Méndez[2], H. González-Martínez[2], M. de J. Perea-Flores[2], S. A. Mendoza-Vázquez[1], L. González-Victoriano[1]
[1]Departamento de Ingeniería Bioquímica, Instituto Politécnico Nacional, Mexico City, Mexico
[2]Centro de Nanociencias y Micro y Nanotecnologías, Instituto Politécnico Nacional, Mexico City, Mexico
Received: April 30, 2024; Accepted: June 18, 2024

Abstract

Convective drying has been widely used for extending the shelf life of foodstuffs as well as for the study of mass and heat transfer phenomena. This contribution aims to conduct a comprehensive study involving mass and heat transfer kinetics, modeling, and evaluation of surface temperatures, shrinkage, and color during the real-time convective drying of potato slices. A tunnel dryer was specially designed to couple digital and thermal cameras to follow the real-time evolution of the surface temperatures, shrinkage, deformation, and color parameters. Drying and thermal kinetics were studied with Fick's second law, Fourier's approach, and semi-empirical mathematical models to obtain effective moisture diffusivity and energy activation to select the best model for describing drying and thermal kinetics. Effective diffusivity coefficients ranged from 6.12×10^{-10} to 9.71×10^{-10} m^2/s, the activation energy was 13.79 kJ/mol, while Page's model and an exponential function of three parameters were shown to be suitable for modeling drying and thermal kinetics. In addition, morphometric and color parameters obtained in real-time help select the best drying conditions and final product quality. This contribution provides essential information for a fuller understanding of the drying, design, and operation of drying equipment for food materials.
Keywords: Semi-empirical models, thermal kinetics, image analysis, deformation, quality parameters.

Resumen

El secado por convección se ha utilizado ampliamente para prolongar la vida útil de alimentos, así como para el estudio de los fenómenos de transferencia de masa y calor. Esta contribución tiene como objetivo realizar un estudio exhaustivo de la cinética de secado, el modelado matemático y la evaluación de las temperaturas superficiales, la contracción y el color durante el secado convectivo en tiempo real de rodajas de papa. Se diseñó un secador de túnel para acoplar cámaras digitales y térmicas para seguir la evolución en tiempo real de las temperaturas de las muestras. El secado y la cinética térmica se estudiaron con la segunda ley de Fick, enfoque de Fourier y modelos matemáticos semi-empíricos para obtener una difusividad de humedad efectiva y activación de energía para seleccionar el mejor modelo para describir el secado y la cinética térmica. Los coeficientes de difusividad efectiva variaron de 6.12×10^{-10} a 9.71×10^{-10} m^2/s, la energía de activación fue de 13.79 kJ/mol, mientras que el modelo de Page y una función exponencial de tres parámetros se mostraron adecuados para su modelado. Además, los parámetros morfométricos y de color obtenidos en tiempo real ayudan a seleccionar las mejores condiciones de secado y la calidad del producto final. Esta contribución proporciona información esencial para una comprensión más completa del secado, el diseño y el funcionamiento de los equipos de secado de materiales alimentarios.
Palabras clave: Modelos semi-empíricos, cinética térmica, análisis de imagen, deformación, parámetros de calidad.

*Corresponding author. E-mail: jchanona@ipn.mx;
https://doi.org/10.24275/rmiq/Alim24322
ISSN:1665-2738, *issn-e*: 2395-8472

1 Introduction

Convective drying is a technology used extensively to dry plant tissues and extend their shelf life (Gaeini *et al*., 2023). Drying technology has been used for the past few decades, but several non-thermal processes and emerging food preservation technologies currently improve final products' quality properties (Cheng *et al*., 2023). However, these food preservation methods require equipment and facilities that are more expensive than hot air dryers, although convective drying is still a reliable technology for producing foodstuffs in huge volumes at low cost. In addition, the higher mass and heat transfer rates that occur with this approach lead to an increased reduction in the water activity of food materials, reaching up to minimal levels (Zhang *et al*., 2021). It also helps to extend shelf life and prevent biochemical reactions and microbial deterioration without special packing or additional preservation methods.

Diverse strategies have been applied to characterize the drying process in a non-steady state. Drying kinetics is the most used approach due to the easy acquisition of moisture data and the straightforward interpretation of curves for describing the drying of food materials. Moreover, several drying studies on thin chips from tubers have been carried out, but potatoes (*Solanum tuberosum*) are among the most used tubers for conducting drying studies and are considered the ideal material due to their high production and consumption, as well as their homogeneous structure and simple composition (Geng *et al*., 2023; Silva Júnior *et al*., 2023). Potatoes are usually dehydrated in cubes and slabs to obtain their drying kinetics and drying rate curves (Wang *et al*., 2020). In contrast, some drying parameters, such as equilibrium moisture, effective diffusivity coefficients, and activation energy, are obtained by applying the classical drying theory, Fick's second law, and the Arrhenius equation (Silva Júnior *et al*., 2023; Valdés-Parada *et al*., 2023). Another approach for evaluating the drying kinetics is using semi-empirical models based on Newton's law of cooling along with logarithmic functions (Raponi *et al*., 2022; Thuy *et al*., 2023). One advantage of the mathematical model's application is that it provides a simplified route for obtaining data and equations for routines to select the drying times in batch cycles, equipment design, and simulations by computer fluid dynamics. Nevertheless, semi-empirical models yield kinetic parameters without physical meaning (Keneni *et al*., 2019).

It is well known that mass and heat transport phenomena simultaneously occur during convective food drying (Mahiuddin *et al*., 2018). Nevertheless, only a few thermal studies have been conducted as it is not possible to measure the temperature of the whole surface material in real-time, even though surface temperature profiles could provide valuable information about the heat transport phenomena during food drying (Traffano-Schiffo *et al*., 2014). After the COVID-19 pandemic, low-cost thermal imaging cameras based on infrared emission are now more available for measuring the surface's temperature. Thus, thermal imaging cameras can assist with the study of food drying and facilitate straightforward temperature measurement of the whole sample surface during drying without the inconvenience of using thermocouples.

Similarly, image analysis has been extensively applied, which helps to evaluate the changes in size, shape, and color in final products and during food processing (Bai *et al*., 2022). These are considered quality parameters for dehydrated foodstuffs, although this approach has only recently been used to describe morphometric and quality changes in real-time. This approach continues to be employed in this context, but more information about their impact on food quality is still needed. Therefore, this work aims to comprehensively study drying, thermal, shrinkage, and color kinetics using digital and thermographic imaging of potato slices under real-time convective drying.

2 Materials and methods

2.1 Potato slices preparation

Potatoes (*Solanum tuberosum*) were selected from a local market in Mexico City, Mexico. Tubers with similar skin color and size and without physical or microbiological damage were chosen carefully. The potatoes were stored in refrigeration at 4 °C. Half an hour before the experiment's preparation, the tubers were removed from refrigeration. Before slice preparation, the samples were carefully cleaned with cold water, and the settings on an electric food slicer (Eura Mod. RIN 2509, Mexico City, Mexico) were adjusted to produce slices 3 mm thick. Subsequently, a stainless-steel cutting mold was employed to cut circles with a diameter of 40 mm. The potato slices were blanched at 90 °C for 5 min and cooled at 4 °C for 2 min by immersion in water (Figure 1a) to avoid enzymatic browning (Naderinezhad *et al*., 2016).

2.2 Drying kinetics

Convective drying kinetics were carried out in an experimental tunnel-type dryer, constructed with internal and external walls of 18-gauge steel sheets and insulated with fiberglass. The tunnel-type drier measured 145 cm in length with a width of 20 cm and a height of 15 cm (Figure 1b). Throughout the process, the dry bulb temperature and airflow were controlled automatically from the equipment's control panel. Furthermore, the wet bulb temperature (T_{wb}) was measured with a thermometer covered in a wet cloth to evaluate the absolute humidity (Y) from a psychrometric chart at 0.77 atm. The airflow is parallel to the sample with an input of absolute humidity at around 0.009-0.006 kg water/kg dry air. For all experiments, three samples were positioned in the inspection area for thermographic and digital imagining acquisition and analysis (Figure 1c).

2.3 Determination of moisture content, effective diffusivity coefficient, and activation energy

The potato slices were weighed using an analytical balance (AZ214, Sartorius, USA), and the samples were recorded at the times indicated by the drying kinetics. For the different samples, three slices were used in the same conditions. The initial moisture content was determined using the AOAC (1999) method, with the moisture content expressed as dimensionless values using equation (1) to obtain the moisture rate (MR) parameter:

$$MR = \frac{M_t - M_e}{M_0 - M_e} \tag{1}$$

Where M_t is the moisture content at any time, M_0 is the moisture content at time zero, and M_e is the moisture content at equilibrium conditions. Over long drying periods, M_e remains constant, and MR can be estimated as Pei *et al*. (2014) expressed in equation (2):

$$MR = \frac{M_t}{M_0} \tag{2}$$

To calculate the effective diffusivity coefficient (D_{eff}) during the falling rate drying period, Fick's second law for slabs was employed (ElGamal & Liu, 2021) as shown in equation (3):

$$MR = \frac{8}{\pi^2}\sum_{n=0}^{\infty}\frac{1}{(2n+1)^2}\exp\left[\frac{(2n+1)^2\pi^2 D_{eff}t}{4L_0^2}\right] \tag{3}$$

Where L represents half the slice's thickness (m), n denotes the number of terms in the diffusion equation, and t is the drying time. Thus, equation (3) can be simplified as follows Akpinar & Toraman (2016) in equation (4):

$$MR = \frac{8}{\pi^2}\exp\left(-\frac{\pi^2 D_{eff}t}{4L_0^2}\right) \tag{4}$$

And equation (4) can be rewritten logarithmically as follows:

$$\ln MR = \ln\frac{8}{\pi^2} - \frac{\pi^2 D_{eff}t}{4L_0^2} \tag{5}$$

Thus, the D_{eff} can be easily determined through the plot of ln (MR) *vs.* t. The slope (m) of this linear relationship was employed to calculate the D_{eff} (Akpinar & Toraman, 2016) as explained in equations (6) and (7):

$$m = -\frac{\pi^2 D_{eff}}{4L^2} \tag{6}$$

$$D_{eff} = \frac{m(4L^2)}{\pi^2} \tag{7}$$

To determine D_{eff}, the actual thickness of the samples was measured using a digital caliper (IP54, Fowler, China). Measurements were taken at the cardinal and center points, resulting in 5 readings per slice (Figure 1a). The average thickness throughout the drying kinetics was calculated from these readings and performed in triplicate for each drying time.

In addition, activation energy could be calculated by using the Arrhenius equation (8) from the linear relationship between the ln (D_{eff}) and the inverse of absolute temperature (Azimi-Nejadian & Hoseini, 2019):

$$D_{eff} = D_0 \exp\left(-\frac{E_a}{RT}\right) \tag{8}$$

Where D_0 is the pre-exponential factor of the Arrhenius equation (m^2/s), Ea is the activation energy (kJ/mol), R is the gas constant (8.3143 kJ/mol), and T is the absolute temperature (Perea-Flores *et al*., 2012). Another strategy for characterizing the drying kinetics is using semi-empirical models, as shown in the following section.

2.4 Modeling of drying kinetics using empirical mathematical models

Therefore, drying kinetics were fitted to five selected thin film drying models to accurately describe the drying process for potato slices (Doymaz, 2017; Perea-Flores *et al*., 2012). The chosen models are based on logarithmic functions and are described below:

Lewis model

The Lewis or Newton model (Equation 9) is the most basic and straightforward model for modeling drying kinetic data in biological products.

$$MR = \exp^{-kt} \tag{9}$$

Page

The Page model is a semi-empirical model derived from Lewis' law, using two constants, as shown in Equation 10.

$$MR = \exp^{-kt^n} \tag{10}$$

Henderson and Pabis

This model corresponds to the initial term in the solution of Fick's second law, making it a two-parameter exponential model in Equation 11.

$$MR = a\exp^{-kt} \tag{11}$$

Logarithmic

This model adapts the Henderson and Pabis model, incorporating an additional constant (Equation 12). Its versatility means it can be applied under various conditions.

$$MR = a\exp^{(-kt)} + c \tag{12}$$

Approximation of diffusion

This model indicates two exponential terms of the mathematical model, as shown in Equation 13.

$$MR = a\exp^{(-kt)} + (1-a)\exp^{-kbt} \tag{13}$$

In the mathematical models, k, n, a, and b are fitting constants, while t is the drying time.

2.5 *Determination of temperatures on the surface of the potato slices*

A thermographic study of the changes that occurred on the surface temperatures during the drying of potato slices is presented as a study model to illustrate that it is possible to promptly estimate the potato slices' thermal kinetics at different temperatures. Similar to those carried out for mass transfer phenomena, empirical models can be applied to describe the food samples' thermal behavior during convective drying.

Thus, to measure the surface temperature of the potato slices in real-time throughout the drying process, two thermographic cameras (IR0280, Perfect Prime, China) were placed in the inspection section to monitor the changes in surface temperature during the drying operation. For this process, the temperatures ranged from -30 to 1000 °C (accuracy ±1 °C), with a spectral range of 8-11.5 mm, a thermal sensor of 32 x 32, a pixel resolution in thermal mode of 3.5 mm/pixel, a resolution digital camera 0.2 Mpx, and an image capturing frequency of 9 Hz. All thermal images were at a constant emissivity of close to 0.95. Following this procedure, the thermographic images of the top and lateral views of the potato slices were acquired (Figure 1c). To evaluate potato slices' surface temperatures, the average values of the top view thermographic images were used to obtain the surface temperature kinetics of the potato slices. For each slice and drying time, 62 measurements were obtained from a thermography camera utilizing the supplier's computer streaming software (available from https://perfectprime.com/pages/manual) and values were recorded by triplicated.

Moreover, the distribution of potato slices' surface temperatures obtained from the thermographic images was analyzed using the entropy (ET) parameter. This value was estimated from the GLCM texture plug-in of the ImageJ software v1.53 (National Institutes of Health, Bethesda, MD, USA), considering that grayscale images correlated with temperature values (Pieniazek & Messina, 2017). In all the cases, three slices were used as replicated samples.

2.6 *Modeling of the surface temperature kinetics*

Similarly to drying kinetics, the surface temperature kinetics of potato slices were fitted using two semi-empirical mathematical models based on Fourier's second law (Khan *et al.*, 2022). The proposed models are exponential equations (14 and 15) named M_1 and M_2 models as follows,

$$T_s = y0 + a(1 - \exp^{-kt}) \tag{14}$$

$$T_s = a + (y0 - a)(\exp^{-kt}) \tag{15}$$

where T_s is the surface temperature of potato slices, a and k are the constants of the models, and t is time.

2.7 *Evaluating the goodness-of-fit of the mathematical models (mass and heat transfer)*

Mean relative percent deviation (E_{MD}), root mean square error (E_{RMS}), chi-square (X^2), and determination coefficient (R^2) statistical parameters were used to evaluate the goodness-of-fit of the mathematical equations for modeling the mass and heat transfer kinetics. These parameters were used to select the most suitable model to characterize potato slices' drying and surface temperature kinetics (Keneni *et al.*, 2019).

$$EMD = \frac{100}{N}\sum_{i=1}^{N}\frac{|MR,\ exp,i - MR,pre,\ i|}{MR,exp,i} \tag{16}$$

$$ERMS = \left[\frac{1}{N}\sum_{i=1}^{N}(MR,\ exp,i - MR,pre,\ i)^2\right]^{\frac{1}{2}} \tag{17}$$

$$\chi^2 = \frac{\sum_{i=1}^{N}(MR,\ exp,i - \overline{MR},pre,\ i)^2}{N-n} \tag{18}$$

$$R^2 = 1 - \left(\sum_{i=1}^{N}\frac{(MR,pre,i - MR,exp,i)^2}{(MR,\ exp,i - MR,exp)^2}\right) \tag{19}$$

Where MR represents the moisture ratio, *pre i* denotes the predicted data for the moisture ratio, *exp i* represents the corresponding experimental data, *N* is the total number of observations, and *n* is the number of constants of the tested mathematical model.

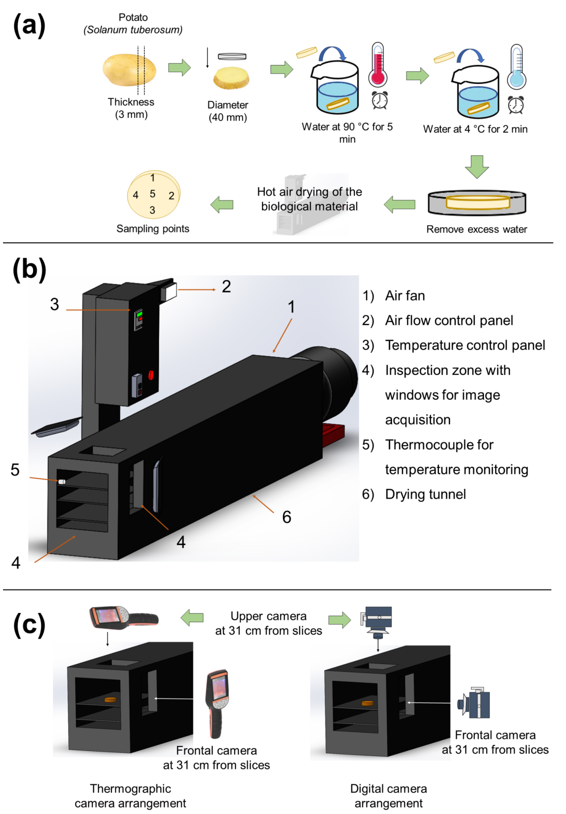

Figure 1. (a) Flow chart describing sample preparation for drying at different times. (b) 3D diagram of the drying tunnel with their parts indicated, (c) Arrangement of digital and thermal cameras to obtain images from top and lateral views during the drying of potato slices.

2.8 *Evaluation of the quality parameters employing image and color analysis*

During potato slice drying, two digital cameras (PowerShot SX110 IS, Canon Inc, China) were used, which were located at 31 cm from the samples to obtain in-situ images from the top and lateral views of the slices (Figure 1c). An LED light ring (Tecnolite, China) of 14 W, daylight, and 26 cm diameter illuminated the section inspection. The obtained images from both the top and lateral views were used to extract specific geometric parameters such as projected area (A), Feret diameter (D), circularity, and color to evaluate the changes in the size, shape, and color of the potato slices during the drying process. Binary images were used for this task, obtained from the original color images, and then converted to a grayscale format using manual thresholding. Previously, the digital cameras were calibrated into the dryer using color charts, as reported by Arzate-Vázquez *et al*. (2011). The original RGB images were converted to CIELab color space using the color space convert plug-in for ImageJ software for the color analysis. In addition, color parameters (L*, a*, and b*) were estimated as average values obtained from

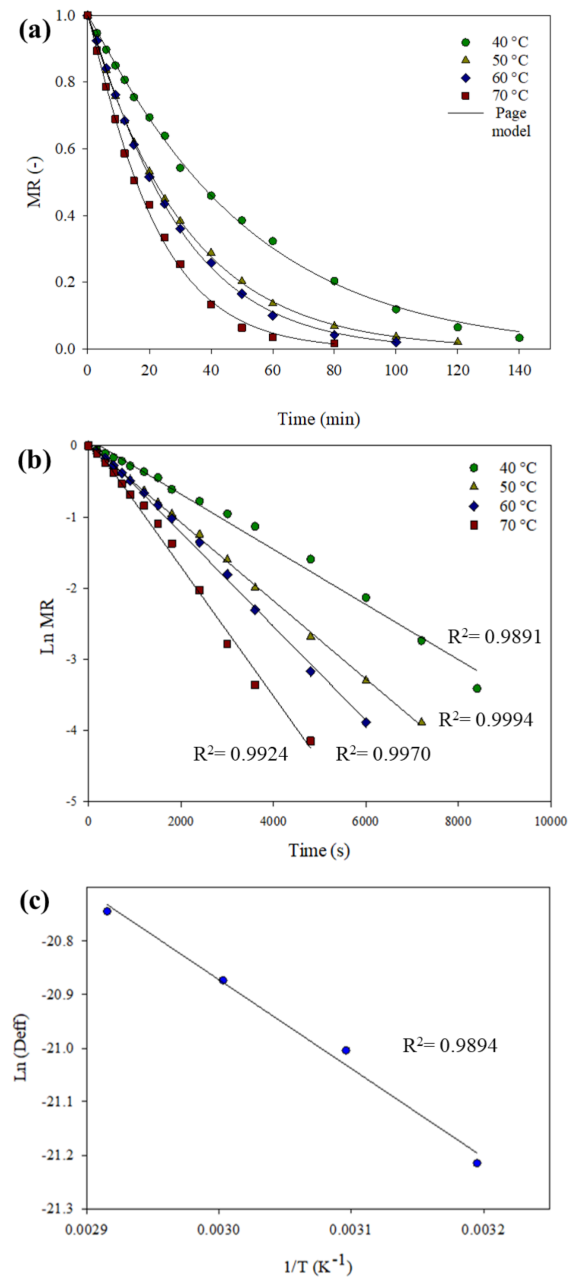

Figure 2. a) Moisture ratio (MR) kinetics, the best mathematical model is indicated (Page model), b) ln (MR) vs. time to evaluate the effective diffusivity coefficient values at different drying temperatures and c) Arrehenius-type relationship for evaluating the energy activation (Ea). Only mean values from three repetitions are shown. Error bars are omitted for a better adjustment.

each separate image and its corresponding frequency histogram. Then, the total color difference (ΔE) was calculated with the following :

$$\Delta E = \sqrt{(\Delta L*)^2 + (\Delta a*)^2 + (\Delta b*)^2} \qquad (20)$$

Where $\Delta L^* = L^* - L_0^*$, $\Delta a^* = a^* - a_0^*$, $\Delta b^* = b^* - b_0^*$, where L*, a* and b_0* are the color parameter values at time t of the drying kinetics, while L_0*, a_0*, and b_0* are color values of the potato slices at the initial time (t_0). The entire image analysis process was carried out using ImageJ software, and all measurements were replicated in triplicate for each sample (Arzate-Vázquez *et al*., 2011; Jaubert-Garibay *et al*., 2023).

2.9 *Statistical analysis*

All modeling and statistical analyses were performed in SigmaPlot v. 15.0 (Systat, Inc. USA).

3 Results and discussion

3.1 *Drying kinetics analysis*

The drying kinetics of potato slices showed the standard dependence on the air-drying temperature (Geng *et al*., 2023; Wang *et al*., 2020). MR kinetics reduced substantially as the drying time elapsed and decreased as the dryer temperature increased. In contrast, the drying time to reach the equilibrium moisture state was diminished with the temperature (Figure 2a). In this study, at 40 °C, the equilibrium condition was reached after 140 min, while at 50, 60, and 70 °C, it was reached after 120, 100, and 80 min of drying, respectively. Similar to those previously reported, these findings are due to the mass transfer's driving force, which significantly increases with drying temperature (Deng *et al*., 2018).

Drying kinetics is observed mainly during the falling drying period (Figure 2a) because the slices are thin with higher airflow (3 m/s), and its dehydration can be described as thin-layer drying (Yi *et al*., 2012), where water diffusion through the food solid matrix is the primary mechanism that controls potato slice drying. For this reason, the effective diffusivity coefficients (D_{eff}) were estimated for different temperature conditions using Fick's second law for slab geometry. Figure 2b shows that the ln(MR) values *vs*. time had a good fit (R^2>0.98) with Fick's second law equation, and the obtained D_{eff} values in function of temperature are presented in Table 1. In particular, the results are similar to the data reported by Silva Júnior *et al.* (2023) for potato cylinders. Lower values were also reported compared to another thermal technology used for potato processing (Table 1).

In addition, D_{eff} values increased as drying temperature increased, and this relationship can be evaluated using an Arrhenius-type equation. Figure 1c shows the linear correspondence between ln (D_{eff}) *vs*. the inverse of the absolute drying temperatures (in K) with an R^2 = 0.9894, with the slope of the plot facilitating the estimation of the activation energy (Ea) necessary for moisture diffusion through potato slices, and equation 21 characterizes this dependence:

$$Deff = 1.59\ x\ 10^{-3} \exp^{\left(-\frac{1659.4}{T}\right)} \tag{21}$$

Where diffusivity constant (D_0) and Ea were 1.59 x 10^{-3} m^2/s of 13.79 kJ/mol, respectively, the obtained Ea values for potato slices were in the reported ranges (10.59–54.93 KJ/mol) for other food materials (Doymaz, 2017; Perea-Flores *et al*., 2012; Thuy *et al*., 2023). The results obtained in the current study regarding drying potato slices at the laboratory level were updated. These are valuable data for understanding drying in a transient state and estimating the time process by batch and scaling of drying equipment in thin food slices.

Table 1. Compares the effective moisture diffusivity of potato samples under various conditions with that in the present study.

Samples	Specific conditions	Effective moisture diffusivity (m^2/s)	Drying conditions	References
Potato slices	40 °C	6.12 x 10^{-10}	Convective dryer at 3 m/s,	This work
	50 °C	7.55 x 10^{-10}	slices with 40-mm diameter	
	60 °C	8.61 x 10^{-10}	and 3-mm thickness	
	70 °C	9.71 x 10^{-10}		
Potato cylinder	40 °C	4.33 x 10^{-10}	Convective drying,	Silva Júnior
	60 °C	8.63 x 10^{-10}	airflow at 0.5 m/s, and	*et al*., (2023)
	80 °C	13.13 x 10^{-10}	equivalent diameter of 1.27 cm	
Potato cylinders	Air impingement drying	0.09 x10^{-9}	Length of 130 mm	Wang
	Infrared heating-assisted	1.18 x 10^{-9}	and diameter of 70 mm.	*et al*., (2020)
	Hot air drying	1.35 x10^{-9}	Hot air at 60 °C	
Potato cubes	40 °C	7.43 x 10^{-9}	Fluidized bed dryer at 1.5 m/s,	Kaveh
	50 °C	8.66 x 10^{-9}	in a range 40 - 70 °C,	*et al*., (2018)
	60 °C	9.25 x 10^{-9}	40 g cubes	
	70 °C	9.76 x 10^{-9}		
Potato slices	200 W	1.55 x 10^{-8}	Microwave oven,	Azimi-Nejadian
	400 W	1.55 x 10^{-8}	thickness of 3.5 mm	& Hoseini,
	600 W	2.20 x 10^{-8}		(2019)
	800 W	2.82 x 10^{-8}		

Table 2. Statistical analysis was conducted based on five mathematical models applied to the drying kinetics of potatoes.

Model	Temperature (°C)	Constants						d	E_{RMS}	X^2	R^2
Lewis	40	k:	0.023					11.895	0.058	0.0031	0.9971
	50	k:	0.032					3.089	0.018	0.0004	0.9989
	60	k:	0.034					13.274	0.054	0.0031	0.9963
	70	k:	0.045					19.212	0.061	0.0044	0.9932
*Page	40	k:	0.015	n:	1.069			6.952	0.039	0.0015	0.9979
	50	k:	0.029	n:	1.031			2.093	0.017	0.0003	0.9992
	60	k:	0.024	n:	1.101			2.597	0.014	0.0002	0.9990
	70	k:	0.033	n:	1.108			7.270	0.034	0.0015	0.9961
Henderson and Pabis	40	a:	1.047	k:	0.020			10.614	0.053	0.0028	0.9946
	50	a:	1.012	k:	0.032			2.350	0.018	0.0003	0.9991
	60	a:	1.027	k:	0.035			10.336	0.040	0.0019	0.9975
	70	a:	1.025	k:	0.047			16.154	0.053	0.0036	0.9942
Logarithmic	40	a:	1.065	k:	0.018	c:	-0.062	2.238	0.026	0.0007	0.9973
	50	a:	1.016	k:	0.032	c:	-0.006	3.089	0.018	0.0004	0.9992
	60	a:	1.054	k:	0.032	c:	-0.036	7.434	0.026	0.0008	0.9985
	70	a:	1.025	k:	0.047	c:	9.49×10^{-13}	16.368	0.042	0.0024	0.9958
Diffusion	40	a:	1.112	k:	0.042	c:	-0.042	2.109	0.025	0.0007	0.9963
	50	a:	1.019	k:	0.033	c:	450.228	1.994	0.014	0.0002	0.9993
	60	a:	-96.774	k:	0.022	c:	1.004	7.776	0.029	0.0011	0.9984
	70	a:	-144.474	k:	0.029	c:	0.029	14.452	0.038	0.0020	0.9961

*Denotes the best-fitting model that aligns with the experimental kinetics.

3.2 Semi-empirical mathematical models applied to dry kinetics

Fick's second law has been widely applied to understand the drying phenomena and obtain Deff values at different temperatures when the entire food drying process occurs during the falling rate period (Doymaz, 2017; Silva Júnior *et al.*, 2023; Thuy *et al.*, 2023). However, its application requires several assumptions and simplifications, such as considering regular geometries (sphere, cylinder, and slabs), neglect shrinkage, constant water diffusivity, homogeneous temperature distribution on the surface and into samples, and when the drying kinetics occasionally show a non-Fickian behavior, remarkable bias can be observed between the experimental and calculated data (Mühlbauer & Müller, 2020; Valdés-Parada *et al.*, 2023).

Alternatively, semi-empirical mathematical models derived from Newton's law of cooling can be used to quickly characterize the drying kinetics, thereby avoiding the restrictions of the Fickian models. The drying kinetics of potato slices were modeled using different mathematical functions, and the results are presented in Table 2. All applied models showed an excellent fit, and high determination coefficient values (R^2>0.99) were found. However, the other goodness-of-fit parameters showed more comprehensive variation ranges than R^2 values. Thus, E_{MD} ranged from 19.77 to 1.99, E_{RMS} ranged between 0.062 and 0.014, and X^2 varied from 0.0040 to 0.0002. These data meant that the best semi-empirical mathematical model for evaluating drying kinetics behavior was selected. Thus, considering all goodness-of-fit parameters, the Page model was selected as the best model to fit drying curves at different temperatures as it showed the lowest bias compared with other mathematical models. Additionally, this model is characterized by its simplicity compared to other models, except for the Lewis model.

Figure 2a shows the experimental MR data fitted to the Page model, and a strong connection can be seen between experimental and model-derived data. However, this approach only involves a mathematical fit of the experimental data without considering the diffusion drying mechanism, while the obtained parameters have no physical meaning (Mühlbauer & Müller, 2020). Only k represents a drying coefficient that usually increases with drying temperature, which can sometimes be linked with the drying rate, as with the D_{eff} values. Even so, these models are helpful because they are straightforward and can be applied without any restrictions imposed by Fick's second law. They could also be beneficial for the modeling and simulating the drying processes.

Moreover, all thin-layer models based on Fick's second law or Newton's law of cooling provide information regarding the changes in the product temperature during drying, an essential parameter in the final quality of dehydrated foods. For this reason, a complementary study of the changes in the samples' surface temperature, size, shape, and color was conducted in real-time better to understand the convective drying of the potato slices.

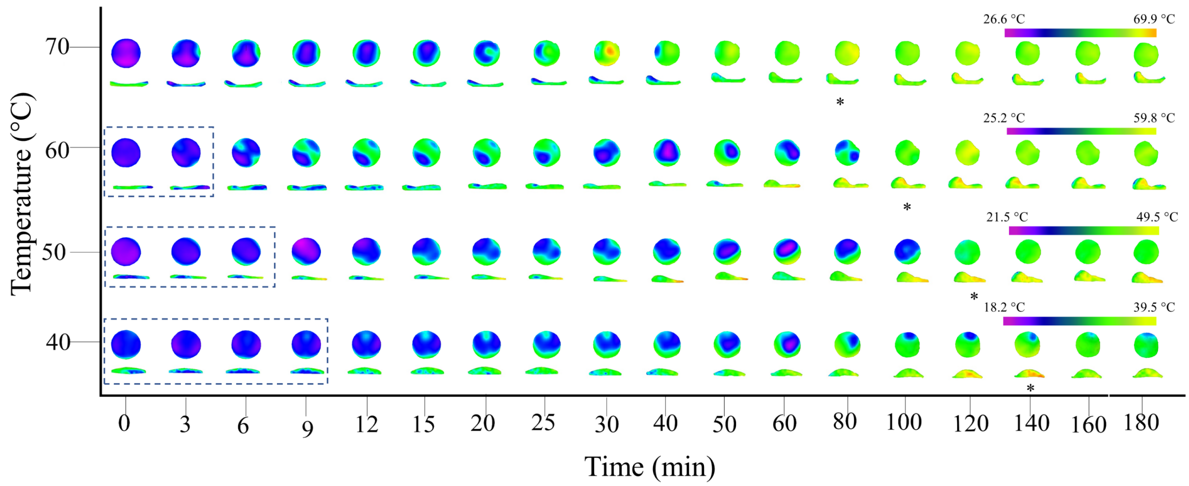

Figure 3. Thermographic images in real time along the drying process of potato slices at 40, 50, 60, and 70 °C. The upper bars correspond to the recorded surface temperature range. *Indicates the time needed to reach equilibrium.

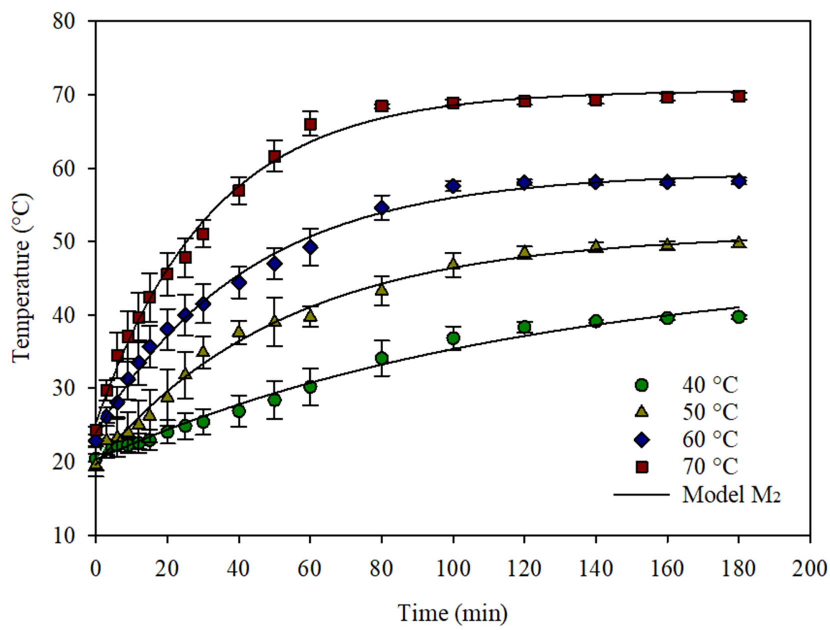

Figure 4. 3D plots of the surface temperatures at selected times (initial, medium, and equilibrium) obtained from thermographic images (to the right of 3D plots) of the potato slices drying at indicated temperatures. ET indicates the entropy of the thermographic images.

3.3 *Analysis of thermographic images*

A selection of the thermographic images of the potato slices during their convective drying at different air-drying conditions is shown in Figure 3. It is clear that the drying temperature influences the surface temperature distribution of potato slices at a low operating temperature (40 °C) during the first 9 min of drying. The whole surface temperatures of the slices remain constant and close to 20 °C (see dashed line in Figure 3), therefore indicating that the surface is water vapor saturated over this period caused by the wet bulb temperature (T_{wb}) of air-drying at 20 °C with a dry bulb temperature of 40 °C (Y= 0.008 kg water vapor/kg air dry). According to the classical drying theory, this period is called the constant rate drying period (Santacruz-Vázquez *et al.*, 2008), where it is expected that the surface temperatures of the slices tend to remain constant, homogenous, and close to the T_{wb} value or the temperature of saturated air. This behavior was also observed at 50 and 60 °C for the air-drying temperature, although the constant rate drying period was reduced to around 6 and 3 min, respectively (see dashed lines in Figure 3). After this period, the slices are dehydrated during the falling rate period, where surface temperatures gradually increase until they reach a temperature close to the air used for drying (40, 50, and 60 °C). The constant drying rate was not detected at 70 °C as the thermal gradient was higher under this drying condition, and water vapor transfer occurred faster than in the other drying conditions studied. Thus, at this temperature, the drying occurs entirely during the falling rate period until it reaches a constant temperature close to thermic equilibrium (70 °C) after 80 min of drying.

Meanwhile, at 40, 50, and 60 °C, the equilibrium temperature is reached after approximately 140, 120, and 100 min thermal processing, respectively (Figure 3). These times are similar to those observed for MR kinetics when reaching the equilibrium moisture, where there is no further mass transfer to the air of the dryer (Figure 2). In all drying conditions during the falling rate period, the surface temperatures showed a heterogeneous distribution where their changes are more drastic at higher drying temperatures (Figure 3) due to initial temperature gradients between slices and drying air.

An analysis of the heterogeneity of the surface temperature distribution is shown in Figure 4. The 3D plots of the surface temperatures at different times (initial, medium, and equilibrium) were obtained from thermographic images of the potato slices (to the right of 3D plots) drying at the indicated temperatures. In this analysis, regions of interest of the 31x31 pixels (on average 62 measurements) from the thermographic images were cropped and converted to grayscale images to be analyzed employing the entropy (ET) parameter. This approach facilitates estimating the image heterogeneity, with high ET values indicating that the pixel's distribution is heterogeneous (Arzate-Vázquez *et al*., 2011). In this case, ET values were associated with the heterogeneity of the surface temperature distribution. Figure 4 shows that during the falling rate period at 30 min, ET values were higher than initial and equilibrium times, indicating that surface temperatures fluctuate more drastically than the constant rate (initial) and equilibrium periods.

Temperature values can also be expressed as thermal kinetics (Figure 5), where it is possible to observe that the standard deviations during the falling rate period were higher than the other two drying periods, which is in line with those observed in the 3D plots and ET values (Figure 4). In addition, the drastic thermal gradients to which the potato slices are exposed during their drying at high temperatures (from 50 to 70 °C) cause severe deformation and shrinkage in the samples (see the lateral view in Figure 3) and heterogeneous distribution of moisture, as has been demonstrated in other studies for food samples and similar drying conditions (Gumeta-Chavez *et al*., 2011; Santacruz-Vázquez *et al*., 2008).

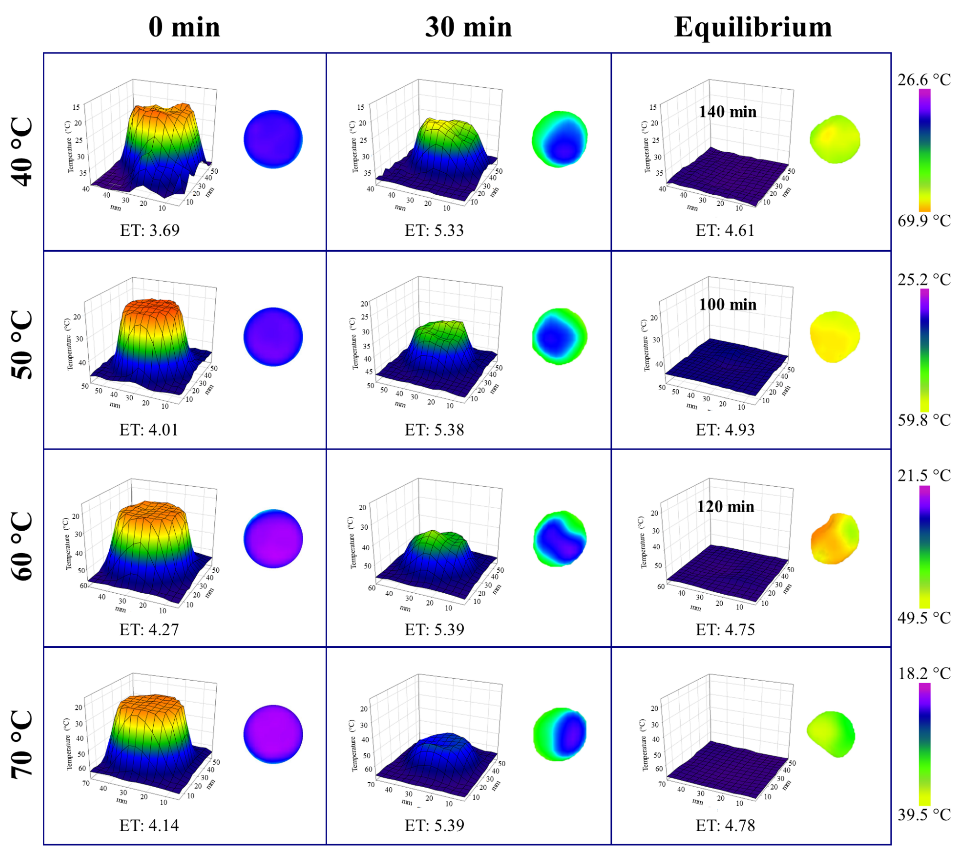

Figure 5. Thermal kinetics of the potato slices when dried at 40, 50, 60, and 70 °C after fitting with the M_2 model.

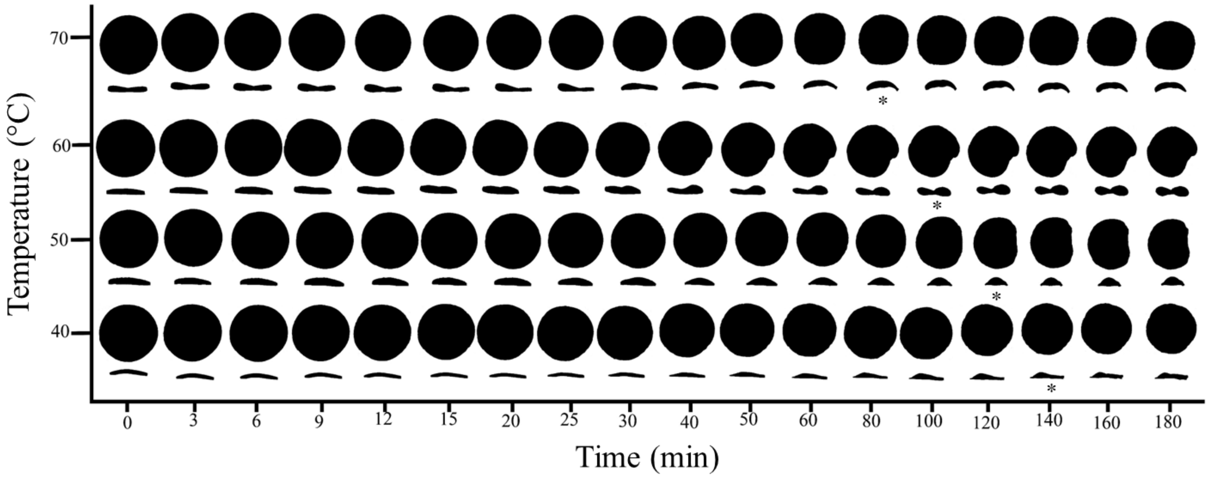

Figure 6. Selected binary images for evaluation of changes in size and shape of the potato slices dried under different temperatures.

Table 3. Statistical results were obtained from the mathematical models based on the second Fourier's law and kinetic parameters for potato slices.

Model	Temperature (°C)	Constants						E_{MD} (%)	E_{RMS}	X^2	R^2
M_1	40	y_0:	20.266	a:	26.815	k:	0.008	2.094	2.883	7.2737	0.9394
	50	y_0:	19.777	a:	31.537	k:	0.018	2.291	3.595	11.3063	0.9996
	60	y_0:	24.022	a:	35.070	k:	0.023	1.775	3.402	10.1256	0.9502
	70	y_0:	25.257	a:	45.308	k:	0.031	1.830	4.216	15.5535	0.977
M_2	40	y_0:	20.266	a:	47.081	k:	0.008	2.094	2.883	7.2737	0.9394
	50	y_0:	19.777	a:	51.314	k:	0.018	2.355	3.595	11.3063	0.9383
	60	y_0:	23.935	a:	59.399	k:	0.023	1.608	3.408	10.1644	0.9661
	70	y_0:	25.257	a:	70.565	k:	0.031	1.665	3.664	11.7459	0.9771

3.4 Modeling of the surface temperatures kinetics

Furthermore, the surface temperature kinetics showed an exponential temperature increase, and its rate increases as the air temperature for drying increases (Figure 6). Two semi-empirical models based on the second Fourier´s law were used to fit the experimental thermal kinetics obtained. The models' performance is presented in Table 3. It can be seen that both models had a good fit and suitable determination coefficient values (R^2>0.938), yet the best performance for evaluating the thermal kinetics behavior was $M_{2,}$ considering the other goodness-of-fit parameters used (E_{MD}, E_{RMS}, and X^2). In addition, k values can be associated with the heat transfer rate for increasing the temperature on the surface of the potato slices during its convective drying. Therefore, k values increased as the air temperature for drying increased. The obtained data could help characterize the surface temperatures during the drying of the potato slices, validate numerical simulations, and implement computer vision systems in situ to inspect the thermal processes of food materials.

3.5 Evaluation of quality parameters in real-time using image analysis

Image analysis has been extensively applied to evaluate the shrinkage and color of dry foodstuffs, although this has usually been limited to final products and without drying equipment (Gomes & Leta, 2012; Jaubert-Garibay *et al.*, 2023). Very few studies have applied image analysis in situ (Bai *et al.*, 2022), even though the monitoring in real-time provides essential information about changes in shape, size, and color during the drying of foods, as well as on quality and phenomenological aspects of drying. Figure 6 shows the changes in size and shape of potato slices for top and lateral views obtained in real-time during the drying process at indicated times and temperatures. Binary images of both views (Figure 6a) show that there is a far more significant presence of shrinkage and deformation at 50 °C and higher drying temperatures (50-70 °C) than at lower temperatures (50 °C). The shrinkage effects on the potato slices are particularly noticeable from the lateral view at 50 and 60 °C. It was also noted that a pronounced folding induced by high-rate mass and heat transfer occurred

(Figures 2a and 5). For the drying at 70 °C, the slices only showed a slight folding in the central zone. The rapid dehydration could have caused crust formation on the surface of the slices, which sealed the surface and hardened the material's structure, reducing its shrinkage and deformation compared with the samples dried at 50 and 60 °C. Meanwhile, at 50 °C, the shrinkage and deformation were less pronounced and more homogeneous because mass and heat transfer rates were slowly controlled (Figure 2a and 5), causing isotropic shrinkage. Previous studies reported these findings for other food materials (mango and agave) that were dried under convective drying and in the form of slices (Gumeta-Chavez *et al*., 2011; Jaubert-Garibay *et al*., 2023).

Image analysis quantifies the morphometric changes in the slices during the drying process; for both views of the project area, Feret diameter, and circularity (geometric parameters) were estimated and expressed as dimensionless values (Figure 7a-f). For the top view, the projected area (A_t/A_0) and Feret diameter (D_t/D_0) decreased exponentially (Figures 7a and 7c).

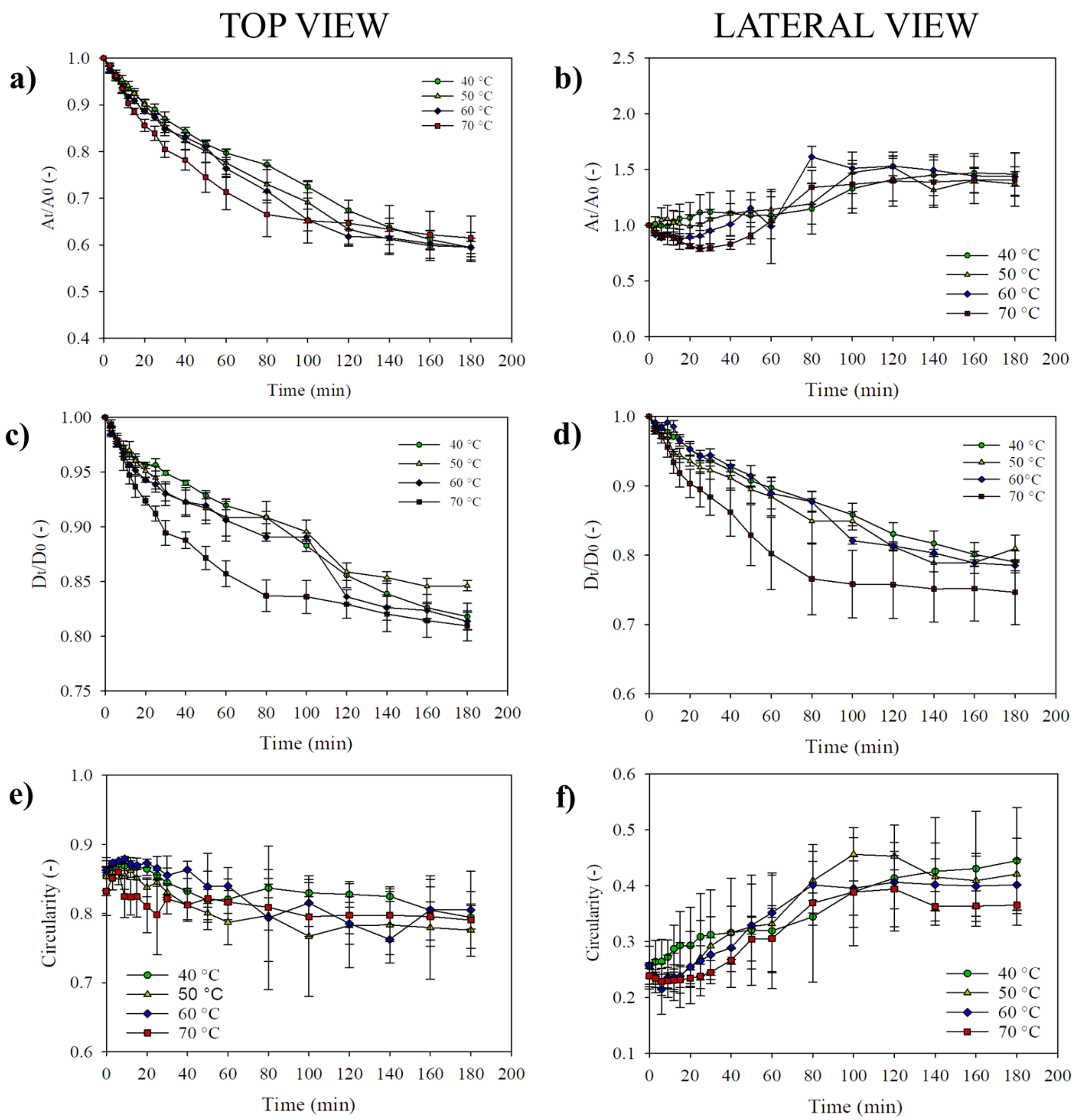

Figure 7. Geometrical parameters evaluated in top and lateral view from binary images: projected area (A_t/A_0), Feret diameter (D_t/D_0), and circularity parameter.

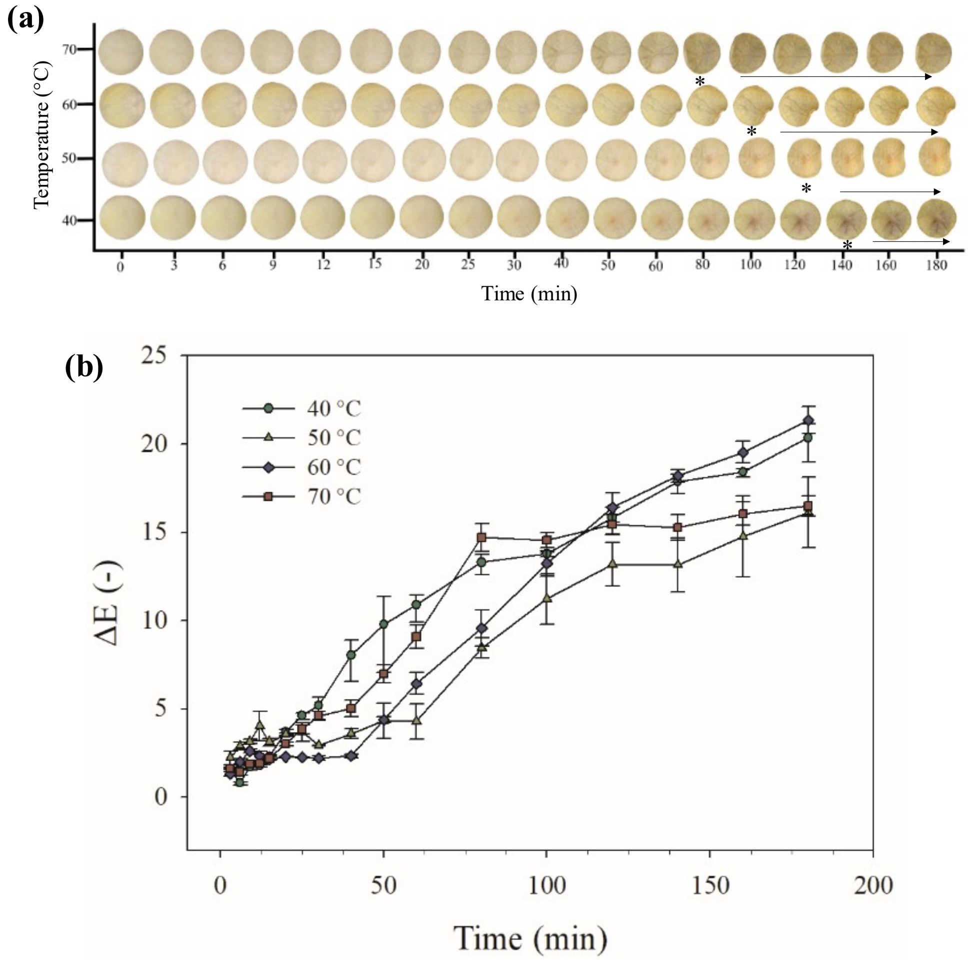

Figure 8. (a) Selected potato slice images during the drying process and (b) total color difference (Δ*E*) changes at indicated temperatures.

At 70 °C, the A_t/A_0 for the top view was slightly lower than other drying temperatures, and it tended to remain constant after around 80 min of drying (Figure 7a). This is similar to what was observed for the drying and temperature kinetics, which may be linked to the occurrence of crust formation. For the lateral view at all temperatures, the A/A0 gradually increased (Figure 7b). In contrast, the Feret diameter showed a considerable reduction for both views at 70 °C (Figures 7c and 7d) due to the deformation and folding of slices caused by thermal stress, anisotropic shrinkage, and the reduced thickness of samples. In the case of 40 °C, the Feret diameter from the top view showed a slight reduction compared with other temperatures (Figure 7c) as it had the lowest drying rate. The circularity parameter is a measure of deformation, the values of which decreased for all studied temperatures in the top view (Figure 7e) while the slices lost their circular shape. From the lateral view, in contrast, the circularity values gradually increased (Figure 7f). As the slices were thin, they folded drastically, especially at 50 and 60 °C (Figure 6). These findings correspond with those reported in other studies related to the same field (Gumeta-Chavez *et al*., 2011). Overall, monitoring the size and shape during drying provided a suitable description of the shrinkage and deformation of the potato slices, the parameters linked to their quality, and the drying rate parameters.

Color is a crucial organoleptic characteristic influencing consumer choice. Therefore, evaluating colorimetric changes in potato slices throughout the drying kinetics is of utmost importance (Wang *et al*., 2020). Figure 8a shows selected color images to illustrate the color changes in real-time of the potato slices during their drying at different temperatures. Only the top views were used for color analysis due to the main area of slices. Despite the blanching of the samples neutralizing browning-causing enzymes during the drying of potato slices, color changes were observed, which may be attributed to non-enzymatic browning, such as carbohydrate caramelization and the Maillard reactions (García-Moreira *et al*., 2024; Leeratanarak *et al*., 2006). Figure 8a shows that at 40 °C, the browning was more pronounced than other drying conditions due to the slow drying rate and the extended processing time required to reach the moisture and temperature of equilibrium. Consequently, more non-enzymatic browning reactions are induced. In contrast, higher drying temperatures (50 and 70 °C) result in less browning in the samples, meaning that fast dehydration produces shorter drying times, minimizing thermal damage and delaying the onset of darkening reactions. Total color change (Figure 8b) during drying was evaluated using ΔE (equation 22) values of the whole slices, where the color changes observed in the color images were quantified. In the case of 60 °C, the excessive shrinkage and deformation induced more browning, and the over-processing produced high ΔE values, considering that the moisture and thermic equilibrium is reached at 100 min.

In summary, geometric and color parameters provide valuable information about product quality and the most suitable time to halt the drying kinetics to avoid over-processing without compromising food quality. These parameters coincide with the times required to reach equilibrium conditions in drying and temperature kinetics. Thus, considering the observed drying rates and temperature kinetics, the time for drying, shrinkage, deformation, and color changes, 70 °C was the most suitable temperature for drying potato slices.

Conclusion

The drying air temperature effect in the 40–70 °C range was studied in potato slices, and their D_{eff} was directly related to temperature increases ranging from 6.12 x 10^{-10} to 9.71 x 10^{-10} m^2/s. In addition, the Arrhenius equation characterized the temperature dependence of D_{eff} values, which yielded an activation energy for moisture diffusion of 13.79 kJ/mol. Drying kinetics were correctly fitted using semi-empirical mathematical models, and Page's model provided the best performance based on statistical comparison parameters such as E_{MD}, E_{RMS}, X_2, and R^2. The thermographic images of the potato slices showed a short, constant rate drying period at 40, 50, and 60 °C. They confirmed that the potato slices were dried for the most part during the falling-rate period, where the moisture transfer was controlled mainly by internal diffusion. Surface temperature profiles for all studied temperatures showed a heterogeneous distribution suitably characterized by entropy parameters. Also, thermal kinetics behavior was well described using semi-empirical models based on Fourier's second law, and an exponential function of three parameters showed the best performance. Image analysis allowed for the characterization of the shrinkage and color changes in real-time, which correlated well with the MR and surface temperature kinetic. These data played an important role in selecting 70 °C as the best temperature for drying the potato slices. The evaluation of in situ drying, thermal, shrinkage, deformation, and color kinetics using thermal and digital imaging could be powerful and non-invasive tools to comprehensively characterize and control the convective drying processes of potato slices in real-time.

This research provides valuable information that could be useful for better understanding mass and heat transfer phenomena that occur during food drying and selecting the best drying times in batch cycles to obtain food products with a controlled quality in real-time. This study will also provide an increased understanding of the design and scaling of drying equipment used for processing food slices and some data suitable for automating the drying process utilizing computer vision systems and for validating thermal phenomena simulations by computer fluid dynamics.

Acknowledgements

SMGM wishes to thank CONAHCyT for the scholarship provided during the author's PhD and the financial support provided by the CONAHCyT projects (239899, 268660), BEIFI, and the Secretaria de Investigación y Posgrado projects at the Instituto Politécnico Nacional in Mexico City in the development of this research (20210065, 20221386, 20230972).

References

Akpinar, E. K., & Toraman, S. (2016). Determination of drying kinetics and convective heat transfer coefficients of ginger slices. *Heat and Mass Transfer/Waerme- Und Stoffuebertragung*, *52*(10), 2271–2281. https://doi.org/10.1007/s00231-015-1729-6

Arzate-Vázquez, I., Chanona-Pérez, J. J., de Perea-Flores, M. J., Calderón-Domínguez, G., Moreno-Armendáriz, M. A., Calvo, H., Godoy-Calderón, S., Quevedo, R., & Gutiérrez-López, G. (2011). Image Processing Applied to Classification of Avocado Variety Hass (Persea americana Mill.) During the Ripening Process. *Food and Bioprocess Technology*, *4*(7), 1307–1313. https://doi.org/10.1007/s11947-011-0595-6

Azimi-Nejadian, H., & Hoseini, S. S. (2019). Study the effect of microwave power and slices thickness on drying characteristics of potato. *Heat and Mass Transfer/Waerme- Und Stoffuebertragung*, *55*(10), 2921–2930. https://doi.org/10.1007/s00231-019-02633-x

Bai, J. W., Dai, Y., Wang, Y. C., Cai, J. R., Zhang, L., & Tian, X. Y. (2022). Potato Slices Drying: Pretreatment Affects the Three-Dimensional Appearance and Quality Attributes. *Agriculture (Switzerland)*, *12*(11). https://doi.org/10.3390/agriculture12111841

Cheng, X., Wang, S., Shahid Iqbal, M., Pan, L., & Hong, L. (2023). Effect of ultrasound-assisted osmotic dehydration on the drying kinetics, water state, and physicochemical properties of microwave vacuum-dried potato slices. *Ultrasonics Sonochemistry*, *99*(July), 106557. https://doi.org/10.1016/j.ultsonch.2023.106557

Deng, L. Z., Yang, X. H., Mujumdar, A. S., Zhao, J. H., Wang, D., Zhang, Q., Wang, J., Gao, Z. J., & Xiao, H. W. (2018). Red pepper (Capsicum annuum L.) drying: Effects of different drying methods on drying kinetics, physicochemical properties, antioxidant capacity, and microstructure. *Drying Technology*, *36*(8), 893–907. https://doi.org/10.1080/07373937.2017.1361439

Doymaz, I. (2017). Drying kinetics, rehydration and colour characteristics of convective hot-air drying of carrot slices. *Heat and Mass Transfer/Waerme- Und Stoffuebertragung*, *53*(1), 25–35. https://doi.org/10.1007/s00231-016-1791-8El

Gamal, R., & Liu, C. (2021). Experimental and simulation study on shrinkage of Radix Paeoniae Alba slices during drying process. *Drying Technology*, *0*(0), 1–12. https://doi.org/10.1080/07373937.2021.1904411

Gaeini, Z., Malmir, H., Mirmiran, P., Feizy, Z., & Azizi, F. (2023). Snack consumption patterns and their associations with risk of incident metabolic syndrome: Tehran lipid and glucose study. *Nutrition and Metabolism*, *20*(1), 1–9. https://doi.org/10.1186/s12986-023-00745-0

García-Moreira, D. P., Moreno, I., Irigoyen-Campuzano, J. R., Martín-Domínguez, I., García-Valladares, O., & López-Vidaña, E. C. (2024). Effect of convective drying on color, water activity, and browning index of peach slices. *Revista Mexicana de Ingeniería Química*, *23*(1), Alim24188. https://doi.org/10.24275/rmiq/Alim24188

Geng, Z., Wang, H., Torki, M., Beigi, M., Zhu, L., Huang, X., Yang, X., & Hu, B. (2023). Thermodynamically analysis and optimization of potato drying in a combined infrared/convective dryer. *Case Studies in Thermal Engineering*, *42*(August 2022), 102671. https://doi.org/10.1016/j.csite.2022.102671

Gomes, J. F. S., & Leta, F. R. (2012). Applications of computer vision techniques in the agriculture and food industry: A review. *European Food Research and Technology*, *235*(6), 989–1000. https://doi.org/10.1007/s00217-012-1844-2

Gumeta-Chavez, C., Chanona-Perez, J. J., Mendoza-Perez, J. A., Terres-Rojas, E., Garibay-Febles, V., & Gutierrez-Lopez, G. F. (2011). Shrinkage and deformation of Agave atrovirens Karw tissue during convective drying: Influence of structural arrangements. *Drying Technology*, *29*(6), 612–623. https://doi.org/10.1080/07373937.2010.514380

Jaubert-Garibay, S., Hernández-Varela, J. D., Chanona-Pérez, J. J., Cárdenas-Pérez, S., Herrera-López, E. J., & Gutiérrez-López, G. F. (2023). Assessing the product quality of mango slices treated with osmotic and microwave drying by means of image, microstructural, and multivariate analyses. *Drying Technology*, *41*(3), 363–377. https://doi.org/10.1080/07373937.2022.2092493

Keneni, Y. G., Hvoslef-Eide, A. K. (Trine., & Marchetti, J. M. (2019). Mathematical modelling of the drying kinetics of Jatropha curcas L. seeds. *Industrial Crops and Products*, *132*(July 2018), 12–20. https://doi.org/10.1016/j.indcrop.2019.02.012

Khan, M. I. H., Batuwatta-Gamage, C. P., Karim, M. A., & Gu, Y. (2022). Fundamental Understanding of Heat and Mass Transfer Processes for Physics-Informed Machine Learning-Based Drying Modelling. *Energies*, *15*(24), 9347. https://doi.org/10.3390/en15249347

Leeratanarak, N., Devahastin, S., & Chiewchan, N. (2006). Drying kinetics and quality of potato chips undergoing different drying techniques. *Journal of Food Engineering*, *77*(3), 635–643. https://doi.org/10.1016/j.jfoodeng.2005.07.022

Mahiuddin, M., Khan, M. I. H., Kumar, C., Rahman, M. M., & Karim, M. A. (2018). Shrinkage of Food Materials During Drying: Current Status and Challenges. *Comprehensive Reviews in*

Food Science and Food Safety, *17*(5), 1113–1126. https://doi.org/10.1111/1541-4337.12375

Mühlbauer, W., & Müller, J. (2020). Drying Atlas. In *Drying Atlas*. https://doi.org/10.1016/c2018-0-02312-9

Naderinezhad, S., Etesami, N., Najafabady, A. P., & Falavarjani, M. G. (2016). Mathematical modeling of drying of potato slices in a forced convective dryer based on important parameters. *Food Science and Nutrition*, *4*(1), 110–118. https://doi.org/10.1002/fsn3.258

Pei, F., Shi, Y., Mariga, A. M., Yang, W. jian, Tang, X. zhi, Zhao, L. yan, An, X. xin, & Hu, Q. hui. (2014). Comparison of Freeze-Drying and Freeze-Drying Combined with Microwave Vacuum Drying Methods on Drying Kinetics and Rehydration Characteristics of Button Mushroom (Agaricus bisporus) Slices. *Food and Bioprocess Technology*, *7*(6), 1629–1639. https://doi.org/10.1007/s11947-013-1199-0

Perea-Flores, M. J., Garibay-Febles, V., Chanona-Pérez, J. J., Calderón-Domínguez, G., Méndez-Méndez, J. V., Palacios-González, E., & Gutiérrez-López, G. F. (2012). Mathematical modelling of castor oil seeds (Ricinus communis) drying kinetics in fluidized bed at high temperatures. *Industrial Crops and Products*, *38*(1), 64–71. https://doi.org/10.1016/j.indcrop.2012.01.008

Pieniazek, F., & Messina, V. (2017). Texture and color analysis of freeze-dried potato (cv. Spunta) using instrumental and image analysis techniques. *International Journal of Food Properties*, *20*(6), 1422–1431. https://doi.org/10.1080/10942912.2016.1211143

Raponi, F., Moscetti, R., Nallan Chakravartula, S. S., Fidaleo, M., & Massantini, R. (2022). Monitoring the hot-air drying process of organically grown apples (cv. Gala) using computer vision. *Biosystems Engineering*, *223*, 1–13. https://doi.org/10.1016/j.biosystemseng.2021.07.005

Santacruz-Vázquez, V., Santacruz-Vázquez, C., Welti-Chanes, J., Farrera-Rebollo, R. R., Alamilla-Beltrán, L., Chanona-Pérez, J., & Gutiérrez-López, G. F. (2008). Effects of air-drying on the shrinkage, surface temperatures and structural features if apples slabs by means of fractal analysis. *Revista Mexicana de Ingeniería Química*, *7*(1), 55–63.

Silva Júnior, M. A. V., Leite, M. A., & Dacanal, G. C. (2023). Modelling of convective drying of potatoes polyhedrons. *International Journal of Food Engineering* , *19*(12), 605–617. https://doi.org/10.1515/ijfe-2023-0016

Thuy, N. M., Giau, T. N., Tai, N. V., & Minh, V. Q. (2023). Drying kinetics and mathematical modeling of dried macaroni supplemented with Gac aril. *Revista Mexicana de Ingeniería Química*, *22*(3), Alim23103. https://doi.org/10.24275/rmiq/Alim23103

Traffano-Schiffo, M. V., Castro-Giráldez, M., Fito, P. J., & Balaguer, N. (2014). Thermodynamic model of meat drying by infrared thermography. *Journal of Food Engineering*, *128*, 103–110. https://doi.org/10.1016/j.jfoodeng.2013.12.024

Valdés-Parada, F. J., Wood, B. D., & Whitaker, S. (2023). Fick's law: A derivation based on continuum mechanics. *Revista Mexicana de Ingeniera Quimica*, *22*(3), Fen23102. https://doi.org/10.24275/rmiq/Fen23102

Wang, H., Liu, Z. L., Vidyarthi, S. K., Wang, Q. H., Gao, L., Li, B. R., Wei, Q., Liu, Y. H., & Xiao, H. W. (2020). Effects of different drying methods on drying kinetics, physicochemical properties, microstructure, and energy consumption of potato (Solanum tuberosum L.) cubes. *Drying Technology*, *39*(3), 418–431. https://doi.org/10.1080/07373937.2020.1818254

Yi, X. K., Wu, W. F., Zhang, Y. Q., Li, J. X., & Luo, H. P. (2012). Thin-layer drying characteristics and modeling of Chinese jujubes. *Mathematical Problems in Engineering*, *2012*. https://doi.org/10.1155/2012/386214

Zhang, W. P., Yang, X. H., Mujumdar, A. S., Ju, H. Y., & Xiao, H. W. (2021). The influence mechanism and control strategy of relative humidity on hot air drying of fruits and vegetables: a review. *Drying Technology*, *1*(1), 1–18. https://doi.org/10.1080/07373937.2021.1943669